The wavenumber-frequency spectrum of free-surface waves in a turbulent, shallow water flow

Giulio Dolcetti[a], Andrew Nichols[a], Kirill V. Horoshenkov[a], Simon J. Tait[b]
[a]Department of Mechanical Engineering, The University of Sheffield, Pitt Street, Sheffield S1 4ET, UK
[b]Department of Civil and Structural Engineering, The University of Sheffield, Mappin Street, Sheffield S1 3JD, UK

Abstract

The characterisation of the dynamic free-surface of a shallow open-channel flow is of considerable interest for many engineering applications since it is related to the transport and mixing processes, particularly near the interface [1]. The rough water surface of open-channels also displays distinctive patterns which are believed to reflect the characteristics of turbulent structures within the flow [2]. In this manner the free surface patterns can be related to the underlying flow conditions [3]. In spite of its importance, the mechanism which leads to the generation of waves at the surface of turbulent flows and the roughness pattern behaviour are still a poorly explored topic.

The wavenumber-frequency spectrum of surface waves defines the spatial and temporal behaviour of the free-surface roughness completely. We suggest an analysis procedure that enables us to determine such spectrum from time series of the surface elevation measured at a set of points distributed non-equidistantly in the flow. The procedure is applied to measured data obtained with an array of conductance wave probes in a rectangular laboratory flume. The results show evidence of the existence of a complex three-dimensional distribution of dispersive gravity waves travelling on the surface. In addition to the dispersive gravity waves, an additional pattern of non-dispersive waves appears to travel at the mean flow surface velocity. This latter type of waves is likely to be generated by the direct interaction with turbulent structures which originate within and are transported by the flow. It is suggested that the application of the proposed method to a wider range of flows will help to clarify the surface-turbulence interaction mechanism, and to define a set of key surface roughness parameters which would simplify the modelling and remote measurement of open channel flows.

Keywords: surface roughness irregular sampling spectrum

1. Introduction

The dynamic behaviour of the rough water surface of shallow turbulent flows is a largely unexplored topic. It is believed that the surface roughness pattern of this type of flows is generated by the interaction between the interface and the turbulence that originates close to the bed [2] although the mechanism of this interaction is still largely unknown. The characteristics of the surface roughness influence the process of transport and mixing [1]. A better understanding of the surface dynamics and its relationship with the flow turbulence would improve the accuracy of transport models and allow for remote monitoring of the flow conditions [3].

Roughness patterns can be generated by the direct action of coherent turbulent structures [2] or by resonant growth of gravity-capillary waves [4]. Turbulence generated structures are found travelling along the flow with the velocity close to the mean surface velocity and independent on the wavelength. Their characteristic dispersion relationship can be written as

$$f(k) = Uk/2\pi \, , \tag{1}$$

Email address: gdolcetti1@sheffield.ac.uk (Giulio Dolcetti)

where f is the frequency in Hz, k is the wavenumber and U is the mean surface velocity of the flow. Gravity-capillary waves can propagate in all directions with velocity equal to the linear superposition of the mean surface velocity and the waves phase velocity. The latter is defined by the gravity-capillary waves dispersive relation

$$c(k) = \sqrt{\left(g + \frac{\gamma k}{\varrho}\right)\tanh(kh)}\ . \tag{2}$$

where g is the gravity constant, γ is the surface tension coefficient, ϱ is the water density and h is the flow mean depth. For the simple case where gravity waves only propagate in the direction parallel to that of the flow, the dispersion relation of waves can be written as

$$f(k) = [U \pm c(k)]k/2\pi\ , \tag{3}$$

where the plus sign represents waves with positive orientation along the flow (advancing) and the minus sign represents waves travelling against the flow (receding).

The generation of surface roughness in a turbulent shear flow has been investigated in [4]. Turbulent structures can generate forced waves with elevation proportional to the magnitude of pressure fluctuations. Forced waves are rapidly dissipated unless their scale and advection velocity matches that of free gravity-capillary waves. When this resonance condition is met, freely propagating waves grow and propagate with a characteristic spatial pattern. When the flow velocity becomes larger than the minimum phase velocity of the waves, $c_{min} = 0.23\ m/s$, long waves propagate at an angle with respect to the mean flow direction, while the pattern of shorter waves remains mainly one-dimensional.

The frequency-wavenumber spectrum of the free-surface roughness uniquely identifies the different roughness patterns based on their dispersion relation. It allows separating the turbulence generated structures from gravity-capillary waves. Frequency-wavenumber spectra of the surface roughness of shallow open channel flows have been measured experimentally [5] and numerically [6, 7]. Both turbulence generated patterns and gravity waves have been observed in these studies. In [5] homogeneous turbulence was generated by means of passive and active grids in an experimental open-channel flume. It was shown that splats and antisplats can generate characteristic patterns on the surface which scale with the size of turbulent structures. These patterns are advected by the mean flow, but rapidly decorrelate because of the propagation of waves in all directions. [6] describes the direct numerical simulation of unsteady open channel flows where turbulence originates at the bottom. Turbulence is found responsible for the generation of forced waves with relatively large wavelength, while shorter free waves propagate according to the gravity-capillary dispersion relationship. Both surface patterns are also observed in [7] for homogeneous turbulence without mean flow. It is suggested that large coherent turbulent structures can generate large surface deformations which in turn can excite patterns of propagating waves especially at low wavenumber. The hypothesis of homogeneous turbulence in [5] and [7] does not apply to real shallow flows where turbulence is generated at the bottom boundary layer. The solution of the direct numerical simulation as in [6] and [7] is time consuming and often impractical, while the experimental method proposed in [5] is limited to experimental flumes and it cannot be adapted to the field.

In this paper the frequency-wavenumber spectra of the free-surface roughness have been measured in a laboratory flume with rectangular cross-section. The surface roughness elevation was measured with an array of conductance wave probes that are irregularly distributed along the flow. The experimental setup can be easily applied to field measurements in order to characterize the free-surface roughness in a variety of realistic conditions. Because of the non-equidistant distribution of the probes, the space-time correlation function needs to be reconstructed on a regular spatial grid before estimating the spatial spectrum. This is done with an interpolation algorithm based on a *sinc* weighing kernel [8, 9]. The accuracy of the reconstruction is improved with an iterative

Email address: gdolcetti1@sheffield.ac.uk (Giulio Dolcetti)

algorithm. The suggested methodology can be applied to a wide variety of laboratory and natural flows due to the flexibility of the wave probes measurement system. The resulting spectra can inform numerical models of the surface that can be of particular interest for modelling of transport and mixing processes or for the development of non-contact monitoring techniques.

2. **Methodology**

2.1. *Definitions*

The flow depth is assumed to be stationary in time and homogeneous in space with average h. The roughness function ζ corresponds to the local variation of the surface elevation with respect to the mean depth h. It is defined in the system of reference (x, y), where x is parallel to the mean flow velocity and the plane $x - y$ lays on the average flat surface. The third dimension, z, coincides with the roughness function ζ. Measurements are taken with one array of sensors positioned along the x-direction. The sensors location is described by $x_j = x_1, x_2, \dots, x_N$, and $y_j = 0$ (along the channel centerline). The sampling rate f_s defines the regular series of time instants $t_k = t_1, t_2, \dots, t_{N_t}$. The space-time correlation function in the x-direction is given by

$$W_x(\rho_n, \tau_m) = \sum_{(u,v)\in\theta(\rho_n)} \sum_k \frac{\zeta(x_u,t_k)\zeta(x_v,t_k-\tau_m)}{N_{\theta(\rho_n)}\sigma^2} \ , \tag{4}$$

where $\theta(\rho_n)$ is the subset of indices with spatial separation $\rho_n = x_v - x_u$ and $N_{\theta(\rho_n)}$ is the numerosity of the subset $\theta(\rho_n)$. σ is the roughness standard deviation, defined as

$$\sigma^2 = \frac{1}{N_x N_t} \sum_j \sum_k \left[\zeta(x_j, t_k)\right]^2 . \tag{5}$$

2.2.*Interpolation on the regular grid*

When the sensors are distributed non-equidistantly, the correlation function is defined for a set of separations ρ_n that are also non-equidistant in general. The estimation of the frequency-wavenumber spectrum of the surface elevation involves calculating the spatial Fourier transform of the correlation function given by equation (4). Because the correlation function is defined on a set of non-equidistant locations, the Discrete Fourier Transform cannot be applied straightforwardly. The finite Fourier series is not orthonormal when defined on an irregular array and this may result in spectral leakage and large spectral variance [8]. These effects can be reduced by interpolating the correlation function $W_x(\rho_n, \tau_m)$ from the non-equidistant spatial grid ρ_n onto a regular grid $\hat{\rho}_r$. The interpolated correlation function is defined as $\widehat{W}_x(\hat{\rho}_r, \tau_m)$. The adopted interpolation method uses the $sinc$ function as a weighing kernel defined on the single dimension ρ for each value of τ_m. The *sinc* kernel gives more accurate results than the Lomb-Scargle periodogram for signals without strong harmonic components [9] and it defines a valid estimator of the correlation function [8]. An iterative algorithm is used in order to minimize the leakage due to non-orthonormality of the $sinc$ base when projected on an irregular grid. At the first iteration

$$\widehat{W}_x(\hat{\rho}_r, \tau_m)^{(1)} = \frac{\sum_n W_x(\rho_n,\tau_m) sinc\left[\frac{2(\hat{\rho}_r-\rho_n)}{\delta\overline{\Delta\rho}}\right]}{\sum_n sinc\left[\frac{2(\hat{\rho}_r-\rho_n)}{\delta\overline{\Delta\rho}}\right]} , \tag{6}$$

where $\overline{\Delta\rho}$ is the size of the target regular grid $\hat{\rho}_r = r\overline{\Delta\rho}$, and δ is a numeric arbitrary coefficient that defines the width of the reconstruction kernel [9]. The reconstruction equation (6) can be inverted in order to estimate the consistence of the first step of the interpolation:

$$W_x(\rho_n, \tau_m)^{(1)} = \frac{\sum_r \widehat{W}_x(\hat{\rho}_r,\tau_m)^{(1)} sinc\left[\frac{2(\rho_n-\hat{\rho}_r)}{\delta\overline{\Delta\rho}}\right]}{\sum_r sinc\left[\frac{2(\rho_n-\hat{\rho}_r)}{\delta\overline{\Delta\rho}}\right]} . \tag{7}$$

Email address: gdolcetti1@sheffield.ac.uk (Giulio Dolcetti)

The error at the κ-th iteration can be estimated as

$$\varepsilon(\rho_n, \tau_n)^{(\kappa)} = W_x(\rho_n, \tau_m)^{(\kappa)} - W_x(\rho_n, \tau_m)\ . \quad (8)$$

The subsequent iterations are defined by

$$\widehat{W}_x(\hat{\rho}_r, \tau_m)^{(\kappa+1)} = \widehat{W}_x(\hat{\rho}_r, \tau_m)^{(\kappa)} - \gamma\hat{\varepsilon}(\hat{\rho}_r, \tau_m)^{(\kappa)}, \quad (9)$$

where γ is an under-relaxation factor that controls the convergence and the correction function $\hat{\varepsilon}(\hat{\rho}_r, \tau_m)^{(\kappa)}$ corresponds to the interpolation of $\varepsilon(\rho_n, \tau_n)^{(\kappa)}$ on the regular grid:

$$\hat{\varepsilon}(\hat{\rho}_r, \tau_m)^{(\kappa)} = \frac{\sum_n \varepsilon(\rho_n, \tau_m)^{(\kappa)} sinc\left[\frac{2(\hat{\rho}_r - \rho_n)}{\delta\overline{\Delta\rho}}\right]}{\sum_n sinc\left[\frac{2(\hat{\rho}_r - \rho_n)}{\delta\overline{\Delta\rho}}\right]}, \quad (10)$$

$$W_x(\rho_n, \tau_m)^{(\kappa+1)} = \frac{\sum_r \widehat{W}_x(\hat{\rho}_r, \tau_m)^{(\kappa+1)} sinc\left[\frac{2(\rho_n - \hat{\rho}_r)}{\delta\overline{\Delta\rho}}\right]}{\sum_r sinc\left[\frac{2(\rho_n - \hat{\rho}_r)}{\delta\overline{\Delta\rho}}\right]}. \quad (11)$$

The iterations can be stopped when the correction $\hat{\varepsilon}(\hat{\rho}_r, \tau_m)^{(\kappa)}$ falls below a given threshold.

2.3. *The frequency-wavenumber spectrum*

Once the space-time correlation function has been interpolated on a regular grid, the frequency-wavenumber spectrum can be estimated by a two-dimensional Fourier transform in space and time

$$S_x(k_p, f_q) = \sum_m \sum_r \widehat{W}_x(\hat{\rho}_r, \tau_m) \exp\left[\sqrt{-1}\left(k_p\hat{\rho}_r - 2\pi f_q \tau_m\right)\right]. \quad (12)$$

3. **Results**

Experimental measurements were performed in a rectangular laboratory open-channel flume at the University of Bradford. The flume is 12.6 m long and 0.459 m wide. The flow discharge and the flume tangent slope can be controlled in order to obtain the desired flow mean depth and velocity. An adjustable gate at the downstream end of the flume ensures that the flow conditions are homogeneous along the open-channel. At the time of measurements the flume bed was covered with a uniform 70 mm thick layer of free randomly distributed gravel. The gravel had mean density 2600 kg/m^3 and characteristic grain size D_{50} = 4.4 mm.

An array of 7 conductance wave probes was installed 10 m downstream from the channel inlet along the flume centerline. Each wave probe was constituted of a pair of 0.24 mm thick tinned copper wires held vertically and anchored to the flume bed below the gravel layer. The two wires that constituted each of the probes were tensioned and aligned perpendicularly to the flow at distance of 15 mm from each other. The array was 480 mm long and the minimum separation between two probes was 30 mm. The locations of all probes with respect to the position of probe n.1 (the one closer to the inlet) are reported in table 1.

Probe n.	1	2	3	4	5	6	7
x-position (mm)	0	130	240	330	400	450	480

Table 1: location of the wave probes

By pairing different combinations of wave probes along the array it is possible to identify 21 unique separations. Of these, two ($\rho_n = 0\ mm$ and $\rho_n = 240\ mm$) are redundant, so that $N_{\theta(0)} = 7$ and $N_{\theta(240)} = 2$. The co-array function $N_{\theta(\rho_n)}$ is represented in figure 1.

Email address: gdolcetti1@sheffield.ac.uk (Giulio Dolcetti)

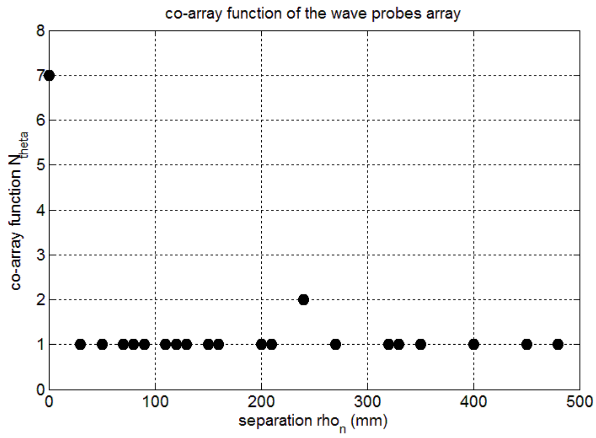

Figure 1: co-array function of the array of wave probes

All the regimes that are reported here have mean depth $h = 100$ mm measured from the top of the gravel bed. The mean surface velocity U was measured by timing the passage of neutrally buoyant floats across a known distance along the flume. U varied between 0.43 m/s and 0.82 m/s as the flume tangent slope increased from 0.001 to 0.004. The single velocities for each regime are reported in table 2 together with the corresponding Froude number $Fr = U/\sqrt{gh}$. For each regime the free-surface elevation was measured contemporarily at each wave probe. The elevation time-series were recorded through a set of Churchill Controls WM1A wave monitors and digitized by a National Instrument PXIe acquisition board with 100 Hz sampling frequency. Each measurement lasted for 30 seconds and was repeated four times for each flow regime. A low-pass third order Butterworth filter with cut-off frequency at 20 Hz was applied to each recorded data set to reduce the eventual electric noise at 50Hz. The filtered data were pruned at both ends to reduce the boundary discontinuity due to filtering. In this way each time series was 28 seconds long. These were then downsampled to 50 Hz effective sampling frequency to reduce the computational cost of the analysis.

Tangent slope	U (m/s)	Fr
0.001	0.43	0.43
0.002	0.65	0.66
0.003	0.70	0.71
0.004	0.82	0.83

Table 2: velocity and Froude number of the tested regimes

Each set was analysed according to the procedure described in section 2. The regular target grid was defined between -240 mm and 240 mm and had grid size $\overline{\Delta\rho}$ = 24 mm. This is smaller than the maximum gap of the irregular grid ρ_n which is equal to 50 mm. The width coefficient of the reconstruction kernel δ was set to $\delta = 2$ after empirical considerations. The smaller value $\delta = 1.5$ made the reconstruction iterative algorithm diverge because of the large gaps in the array ρ_n. The larger value $\delta = 2.5$ produced a marked cut-off of the spatial spectrum at high wavenumber. The reconstruction procedure based on the weighing kernel is found to be associated with low-pass filtering of the reconstructed signal, where δ determines the characteristic cut-off frequency [8]. Therefore, the value of δ must be minimised whenever the high-frequency component of the original signal are of interest.

To avoid divergence of the iterative procedure in its initial stages, the under-relaxation factor γ was set to $\gamma = 0.1$. The iterations were arrested when the maximum over τ_m of

Email address: gdolcetti1@sheffield.ac.uk (Giulio Dolcetti)

$\hat{\varepsilon}(\hat{\rho}_r, \tau_m)^{(\kappa)}$ became smaller than 1% of the maximum of the correlation function $\widehat{W}_x(\hat{\rho}_r, \tau_m)^{(\kappa)}$. Figure 2a shows the maximum of the correction $\hat{\varepsilon}(\hat{\rho}_r, \tau_m)^{(\kappa)}$ for the regime with $h = 100\,mm$ and tangent slope 0.003, as a function of the number of iterations κ. Figure 2b compares the original correlation at 0 time-lag $W_x(\rho_n, 0)$ versus its reconstructed version $\widehat{W}_x(\hat{\rho}_r, 0)^{(\kappa)}$ for the same regime.

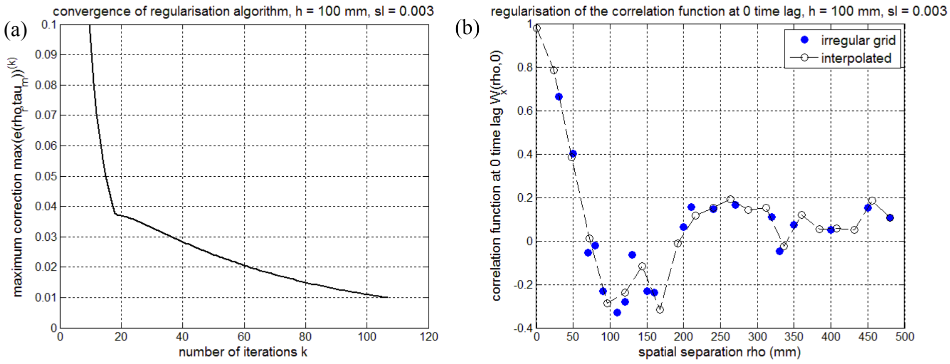

Figure 2: $h = 100\,mm$, tangent slope 0.003. (a) Convergence of the interpolation algorithm. Maximum of the correction $\hat{\varepsilon}(\hat{\rho}_r, \tau_m)^{(\kappa)}$ as a function of the iteration κ. (b) Correlation function at 0 time-lag. Blue dots: measured, on the irregular grid, $W_x(\rho_n, 0)$. Dashed line with circles: reconstructed, after convergence $\widehat{W}_x(\hat{\rho}_r, 0)^{(\kappa)}$.

The wavenumber-frequency spectrum of each flow regime was estimated as the average of the four absolute spectra from each of the 28 seconds long sets. In order to compare the experimental results with the expected dispersion relations of equations 1 and 3 it is necessary to identify the location of the spectral ridges with good resolution. To achieve this, the reconstructed correlation function was zero-padded along the spatial dimension $\hat{\rho}_r$ in both positive and negative direction. The effective size of the spatial array was multiplied by a factor 4, which improves the spectral peak resolution by the same factor. The correlation at the maximum spatial separation $\hat{\rho}_r$ was found smaller than 0.2 for all regimes. This residual correlation would represent a discontinuity at the boundary after zero-padding. Therefore a Hanning window was applied to the correlation function along the spatial dimension $\hat{\rho}_r$ prior to zero-padding.

Figure 3 shows the measured spectra for all the regimes of table 2, together with the expected dispersion relations of turbulence-generated structures and propagating gravity waves (equations 1 and 3). The amplitude of the measured spectra is found decreasing rapidly with the frequency. In order to improve the visualization, the frequency-wavenumber spectra of figure 3 have been divided by the amplitude of the one-dimensional frequency spectrum at each frequency. The function displayed in figure 3 is hence defined as:

$$\bar{S}_x(k_p, f_q) = \frac{S_x(k_p, f_q)}{\frac{1}{2\pi}\int_{-\infty}^{\infty} S_x(k_p, f_q)\, dk_p} \,. \tag{13}$$

The results of figure 3 confirm the capability of the suggested method to estimate the frequency-wavenumber spectra of the surface roughness from a linear array of non-equidistant conductance wave probes. Two main components of the roughness pattern are clearly evident. These are turbulence generated patterns that move at the velocity close to the mean surface velocity, and gravity capillary waves that propagate in both directions parallel to the mean flow following the dispersion relationship of gravity-capillary waves (equation 3). Turbulence generated patterns are more clearly visible in the regime with tangent slope 0.001. For this regime the gravity waves are mainly advancing waves with wavenumber between 50 rad/m and 100 rad/m. As the flume slope is increased, the turbulence generated roughness becomes less distinct and the spectra become dominated by gravity waves. These observations are in agreement with the mechanism suggested in

Email address: gdolcetti1@sheffield.ac.uk (Giulio Dolcetti)

[4] as a slower flow is associated with little elongation of the turbulent structures due to shear. As the velocity increases the growth of resonant waves is promoted as the advection velocity becomes comparable with the phase velocity on a wider range of scales. Receding waves also become more pronounced and they extend to larger positive wavenumber. The negative wavenumber in figure 3 represents waves that propagate towards the negative x-direction. These are receding waves with modulus of the phase velocity larger than the mean surface velocity. Based on the dispersion relationship of equation 3 these waves should be limited to very low frequency and their presence cannot be explained simply by the mechanism suggested in [4].

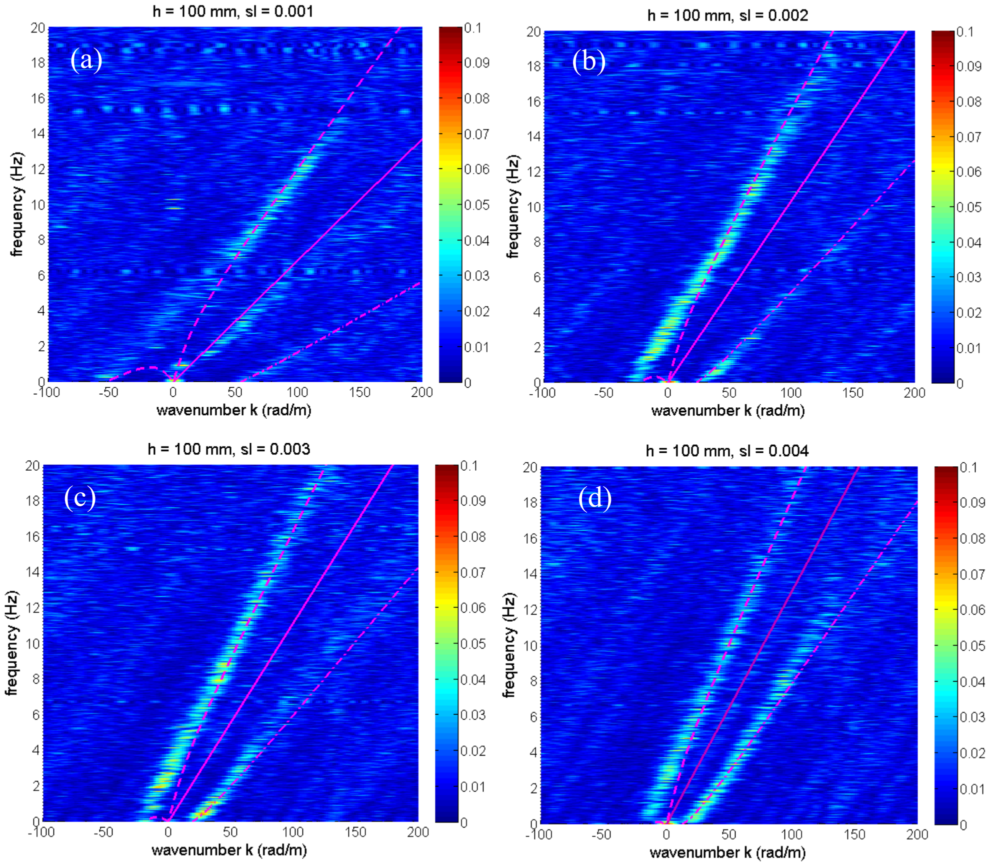

Figure 3: Frequency-wavenumber spectra of the four tested flow regimes with mean depth h = 100 mm. (a) tangent slope 0.001; (b) tangent slope 0.002; (c) tangent slope 0.003; (d) tangent slope 0.003. ————, turbulence generated structures, equation 1; — — — — —, advancing gravity-capillary waves, equation 3; — · — · — ·, receding gravity capillary waves, equation 3.

There is a clear discrepancy between the measurements and the predictions of equation 3 in the low and negative wavenumber range. Equation 3 only accounts for waves propagating parallel to the mean flow. For an arbitrary angle ϑ between the direction of propagation and the flume centerline, it should be written

$$k_x = K \cos\vartheta\,, \tag{13}$$

$$k_y = K \sin\vartheta\,, \tag{14}$$

$$f(K,\vartheta) = [U \cos\vartheta \pm c(K)]K/2\pi\,. \tag{15}$$

Therefore the finite positive value of the dispersion relationship when $k_x = 0$ represents waves propagating along the transverse direction y. Because the wave probes array is distributed along the x-direction only, the wavenumber spectra reported here have been measured with respect to k_x rather than to K, i.e. assuming $\vartheta = 0$. It appears that this assumption is valid for short waves with wavenumber larger than approximately 20

Email address: gdolcetti1@sheffield.ac.uk (Giulio Dolcetti)

rad/m, while longer waves show a more complex two-dimensional pattern that is difficult to understand from measurements in one single dimension. $K = 20$ rad/m corresponds to about three times the mean depth. Waves longer than this are unlikely to be able to propagate along the flume, and it appears reasonable that their relatively large contribution to the wavenumber frequency spectrum comes from shorter waves with different direction of propagation. This is also in agreement with the theoretical model in [4], where it is shown that when the flow velocity exceeds the minimum phase velocity of gravity waves the angular distribution of longer waves becomes bimodal. The resonance condition is only met for waves propagating at an angle ϑ different from zero, while shorter waves remain mainly one-dimensional.

4. **Conclusions**

It has been shown that the frequency wavenumber spectrum of the free-surface roughness of shallow water flows can be measured with good spectral resolution with a linear array of conductance wave probes distributed non-uniformly along the flow direction. The correlation function needs to be interpolated on a regular grid in order to obtain accurate representations of the spectrum. This was done successfully with a weighed binning iterative algorithm based on the *sinc* kernel. The method was tested experimentally on a laboratory flume with homogeneous gravel bed. The tested flows had the same mean water depth $h = 100\,mm$ while the mean surface velocity varied between 0.43 m/s and 0.82 m/s. The results prove that there are patterns of the surface roughness that travel at the velocity close to the mean surface velocity. These patterns are believed to originate from the direct interaction of the free-surface with the large turbulent structures within the flow. The wavenumber-frequency spectra also show evidence of dispersive gravity-capillary waves that propagate on the free-surface whilst being advected at the mean surface velocity. The shortest waves propagate mainly along the flow direction, while it is suggested that long waves should follow a more complex two-dimensional pattern. It is observed that within the range of regimes tested the turbulence generated structures tend to dominate the spectrum when the velocity is low. The impact of gravity-capillary waves increases as the velocity is increased, and receding waves become progressively predominant.

The methodology reported here can be used effectively and accurately in order to determine the dynamic properties of the water free-surface of shallow flows in a variety of conditions. Hence, it would help clarify the behaviour of the free-surface and the mechanism of interaction with turbulence for this type of flows. The correct understanding of these phenomena is fundamental in order to model transport and mixing processes that are strongly influenced by the free-surface characteristics [1] and to develop non-contact techniques for monitoring of the flow conditions [3]. The application of traditional numerical methods to predict the surface deformation based on the direct solution of the hydraulic Navier-Stokes equations is challenging because of the large computational cost. The wavenumber-frequency spectrum that have been presented here can constitute the basis for a more simple type of models where the free-surface dynamic behavior is modelled based on the measured dispersion relationships [10].

5. **References**

[1] Lakehal D., et al. Direct numerical simulation of turbulent heat transfer across a mobile, sheared gas-liquid interface, Journal of Heat Transfer 125(6), 1129-1139, 2003.

[2] Fujita I., et al. Advection features of water surface profile in turbulent open-channel flow with hemisphere roughness elements, Visualization of Mechanical Processes 1(4), 2011.

[3] Horoshenkov, K.V., et al. The pattern of surface waves in a shallow free surface flow, Journal of Geophysical Research: Earth Surface 118(3), 1864-1876, 2013.

[4] Teixeira, M., Belcher, S. On the initiation of surface waves by turbulent shear flow,

Email address: gdolcetti1@sheffield.ac.uk (Giulio Dolcetti)

Dynamics of atmospheres and oceans 41(1), 1-27, 2006.

[5] Savelsberg, R., Van De Water, W. Experiments on free-surface turbulence, Journal of Fluid Mechanics 619, 95-125, 2009.

[6] Borue, V., et al. Interaction of surface waves with turbulence: direct numerical simulations of turbulent open-channel flow, Journal of Fluid Mechanics 286, 1-23, 1995.

[7] Guo, X., Shen, L. Interaction of a deformable free surface with statistically steady homogeneous turbulence, Journal of Fluid Mechanics 658, 33-62, 2010.

[8] Stoica, P., Sandgren, N. Spectral analysis of irregularly-sampled data: paralleling the regularly-sampled data approaches, Digital Signal Processing 16(6), 712-734, 2006.

[9] Rehfeld, K., et al. Comparison of correlation analysis techniques for irregularly sampled time series, Nonlinear Processes in Geophysics 18, 389-404, 2011.

[10] Dolcetti, G., et al. The spectrum of the acoustic waves backscattered by the dynamic rough surface of a shallow water flow, Proceedings of the Institute of Acoustics, 36(3), 422-429, 2014.

Email address: gdolcetti1@sheffield.ac.uk (Giulio Dolcetti)